processes

MDPI

Article

Junction Temperature Prediction Model for GaAs HBT Devices Based on ASO-ELM

Xiaohong Sun *, Yijun Yang and Chaoran Zhang

School of Electronic and Information Engineering, Suzhou University of Science and Technology, Suzhou 215009, China
* Correspondence: zixuan19861002@126.com

Abstract: In this study, an accurate temperature prediction model is proposed for GaAs HBT, which considers both the bias voltage and current rather than power consumption only. The increase in temperature is closely related to the heat source property, which leads to a complex interaction between the lattice vibration and the uneven distribution of the electric field and current density. To improve the accuracy and stability of the temperature prediction model, a machine learning method of Extreme Learning Machine (ELM) optimized with an Atomic Search Algorithm (ASO) is introduced. The validity of the model is verified by comparing it with experimental observations by the QFI InfraScope TM temperature mapping system. The predicted temperatures for an 8 × 8 HBT power cell fabricated with 2 μm GaAs technology show good agreement with the measurement results, with a ±2 °C error and a relative error deviation below 3%. This demonstrates the superior performance of the proposed model in accurately predicting the temperature of GaAs HBT.

Keywords: GaAs HBT; junction temperature; ELM; ASO; power cell

Citation: Sun, X.; Yang, Y.; Zhang, C. Junction Temperature Prediction Model for GaAs HBT Devices Based on ASO-ELM. *Processes* **2023**, *11*, 1346. https://doi.org/10.3390/pr11051346

Academic Editor: Giampaolo Manzolini

Received: 24 March 2023
Revised: 20 April 2023
Accepted: 25 April 2023
Published: 27 April 2023

1. Introduction

GaAs HBTs are widely used in the design of RF power amplifiers due to their excellent power processing ability at high frequencies. However, high-performance power amplifier design typically involves a trade-off between efficiency and linearity, resulting in high power consumption. This, in turn, leads to significant heating effects in the active transistors, especially with increasing integration. The low thermal conductivity of 45 W/(m·K) of GaAs material exacerbates the issue of temperature increase during operation [1]. This increase in temperature has a detrimental impact on the reliability of the circuit and can even cause the device to burn out. As a result, it is crucial to accurately predict the maximum junction temperature of the device to improve the effectiveness of heat treatment, thermal compensation, device package design, and system cooling requirements [2]. Accurate temperature prediction is particularly important as device integration increases. A temperature prediction model that considers the bias voltage and current, rather than just power consumption, is essential for effective heat management.

The direct method [3] for temperature acquisition is inseparable from expensive optical instruments. While the indirect method for temperature acquisition mainly relies on finite element simulation and mathematical calculation methods. A finite element simulation is typically implemented using software such as Silvaco, COMSOL, or ANSYS [4]. This complex process involves several steps, including device structure definition, mesh division, and physical and boundary condition definitions. It is a time-consuming process that requires careful attention to ensure the validity and convergence of the solution. Mathematical calculation methods use thermal resistance to establish relationships between steady temperature and power consumption. The thermal conduction angle is an effective intermediate variable for deriving the equivalent thermal resistance based on the heat source and boundary conditions. In power cells constructed using multiple fingers in modern power amplifier designs, the spacing between fingers, the location and geometry

of the active area, and metal interconnections all influence the thermal conduction angle [2]. In the literature [5], the authors presented a method to estimate the junction temperature and thermal resistance of HBTs by analyzing the temperature dependence of thermal conductivity. This approach is flexible enough to be applied to various structures and processes, whether they include trench isolation and metal layers or not. However, it may not be appropriate for materials with non-linear temperature dependence of thermal conductivity, which must be precisely measured, especially at high temperatures. To address this issue, a new method to calculate the junction temperature, which better accounts for the non-linear variation of thermal conductivity, was introduced in the literature [6]. This method is applicable to different semiconductor materials and device structures. However, it overlooks the influence of other factors inside the device on the junction temperature, such as current density and electric field distribution. On the other hand, the temperature dependence of the current gain of the transistor can also be used as an effective variable for calculating the junction temperature. In the literature [7], the authors used the RF signal to correct the power dissipation of the transistor and estimated the junction temperature and thermal resistance of the transistor by analyzing the thermal dependence of the current gain. Nevertheless, accurate calibration of the RF signal generator and current gain measurement system is necessary, and the method is susceptible to noise or interference from other sources in the RF signal or current gain measurement. As output power increases, the maximum temperature is affected by higher-order effects of power consumption and is corrected using a non-linear expression of power series. The above methods are based on polynomials that assume power consumption is the only excitation factor leading to an increase in junction temperature. However, according to the literature [8], when analyzing lattice heating with the electric field and current density distribution under a fixed bias voltage, the center of the heat source will drift with increasing current. Consequently, the device temperature is presumed to be voltage and current-dependent rather than solely dependent on their production. Therefore, a temperature prediction model that considers bias voltage and current is more accurate than one based solely on power consumption.

The conventional methods above are physics-based and require knowledge of the thermal parameters, such as the thermal conductivity and heat capacity of the HBT, as well as the geometry and material properties of the device. Then, they apply methods, such as thermal networks or finite elements, to solve the thermal equations and obtain the junction temperature and thermal resistance. Neural networks are a more versatile and robust tool that can establish highly nonlinear and complex relationships through training data without requiring explicit mathematical expressions. Therefore, neural networks have been increasingly used by researchers in the field of microelectronic device junction temperature calculation. In this regard, BP neural network is one of the most commonly used methods. It has a powerful nonlinear mapping ability and can be trained by a backpropagation algorithm. Literature [9] constructed an IGBT junction temperature prediction model using this advantage of the BP neural network and achieved better prediction accuracy than polynomial fitting methods. However, BP neural network also has some disadvantages. For example, it may cause overfitting during the training process and require a large amount of computing resources and time. Moreover, its prediction accuracy is affected by network structure and parameters, which need to be constantly manually adjusted to obtain the best results. To overcome these problems, some researchers have explored other types of neural network models. For example, literature [10] combined BP, interpolation and Kalman filtering to further improve the accuracy of neural networks in IGBT junction temperature prediction. Literature [11] proposed a knowledge-based neural network (KBNN) method that further reduces the computational complexity of modeling. KBNN method uses basic physical principles to constrain the structure and parameters of neural networks and can optimize network performance through adaptive learning. In contrast, an extreme learning machine only needs to set the number of nodes in the hidden layer of the network and does not require adjustment of the input weights and biases of the hidden layer nodes during the algorithm execution in order to produce a unique optimal solution [12,13]. Therefore, it has

the advantages of fast learning speed and good generalization performance. Its disadvantage lies in that the accuracy of the model depends on the input weights and thresholds. To improve the stability and accuracy of the ELM model, intelligent optimization algorithms are usually used to determine the optimal weight and threshold parameters of the network. Literature [14] used the particle swarm algorithm (PSO) to optimize the parameters of ELM and achieved accurate results in estimating daily evapotranspiration. Literature [15] proposed using the genetic algorithm (GA) to optimize ELM for modeling the relevant characteristics of GaN pseudomorphic high electron mobility transistor (P-HEMT) large signals. The GA algorithm is complex to encode, has insufficient local search capability and random wandering phenomenon, and relies on empirically selected parameters to influence the optimal solution. Moreover, the convergence and search efficiency of the algorithm is poor. Another popular optimization method is the PSO algorithm, which converges quickly but easily gets stuck in local optima. Therefore, it is prone to premature convergence. Recently, a new optimization method called Atomic Search Optimization (ASO) was proposed [16]. This method has fewer adjustable parameters and better search capability than GA and PSO. The ASO algorithm uses the gravitational force and the repulsive force between atoms to motivate them to explore space more extensively and efficiently. The ASO algorithm has fast convergence and strong search ability, which can significantly improve the efficiency of solving complex problems. In this work, we use the ASO algorithm to optimize ELM and construct the ASO-ELM model to predict the junction temperature of GaAs HBT transistors.

This paper presents a constructed ELM model that takes bias voltage and current as inputs and junction temperature as output. The ASO algorithm is utilized to optimize the input weights and hidden layer thresholds of the model to establish the optimal combined model. To validate the effectiveness of the model, actual temperature measurements were conducted using a 2W HBT power cell with the QFI InfraScope TM temperature mapping system. The results indicate that the proposed model accurately and reliably predicts the maximum junction temperature of the devices.

2. Measured Devices and Data Processing

2.1. Measured Devices

The power cell is comprised of 64 HBTs, where each HBT's emitter area is 80 μm^2. The substrate has a 100μm thickness [17]. Two backside thermal vias (BTVs) are situated between two adjacent transistor arrays. The bare slice area measures 1100 μm × 690 μm. Figure 1 shows the temperature distribution measured by the QFI infrared device at U_{ce} = 5 V, I_c = 400 mA, and a fixed substrate temperature of 75 °C. Under steady operation conditions, the lowest temperature is 83.36 °C, and the highest temperature reaches 171.49 °C.

2.2. Data Processing

To ensure the temperature measurement system's accuracy, the power cell's substrate temperature on the test bench is fixed at 75 °C. The device is connected to two power sources and operated in the forward state. The collector bias voltage V_c is initially set at 4 V, and the base voltage V_b is adjusted to alter the base current Ib. Subsequently, the collector current I_c varies from 100 mA to 600 mA with an increment of 5 mA. When the device reaches a steady state temperature, the corresponding V_c and I_c are used to determine the maximum junction temperature at the center. This process is then repeated for collector bias voltages of 5 V and 6 V. To minimize the influence of data noise and dimensionality; the maximum and minimum norm method is employed to normalize the input and output data within the range of [0,1]. Following the elimination of outliers, a total of 293 sets of actual data, comprising collector bias voltage, collector current, and corresponding maximum junction temperature data, are obtained. Finally, 270 training samples are designated as training sets, and 23 samples are set aside as test sets.

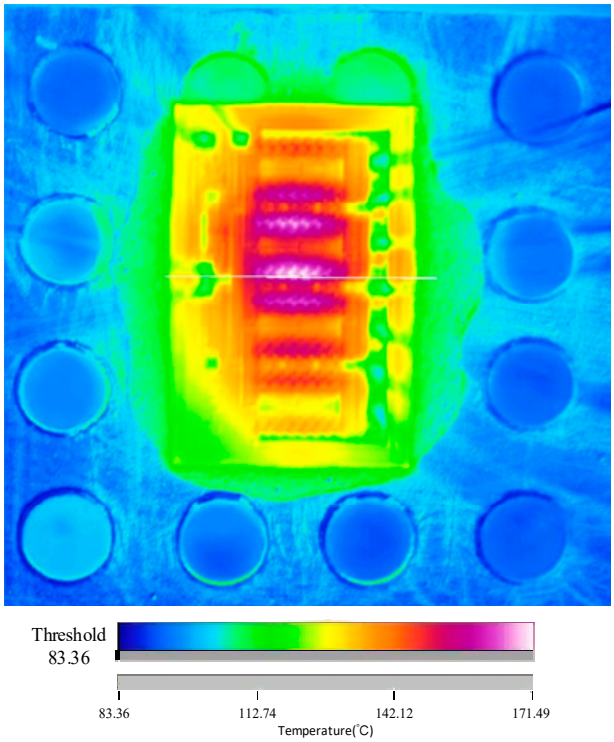

Figure 1. Temperature distribution diagram of QFI.

3. Method

3.1. ELM Principle

ELM [18] is a feedforward neural network with a single hidden layer that determines the output weight matrix using a generalized inverse approach rather than an iterative approach. In contrast to traditional BP neural networks, ELM has a simpler structure and trains considerably faster. During the training process, the connection weights of the input and hidden layers and the hidden layer threshold are randomly generated and do not require pre-setting, reducing the need for human intervention. The only parameter that must be established is the number of neurons in the hidden layer to obtain the optimal solution under specific conditions.

For Q arbitrarily different samples (x_i,y_i), $x = [x_{i1},x_{i2}, \ldots, x_{in}]^T \in R^n$, $y_i = [y_{i1},y_{i2}, \ldots, y_{im}]^T \in R^m$, a single hidden layer feedforward neural network with L neurons can be represented as

$$\begin{aligned} &\sum_{i=1}^{L} \beta_i g(a_i x_j + b_i) = u_j \\ &i = 1,2,\ldots,L, j = 1,2,\ldots,L \end{aligned} \tag{1}$$

where $a_i = [a_{i1}, a_{i2}, \ldots, a_{in}]^T$ is the input weight, b_i is the bias of the i-th hidden layer neuron, $x_j = [x_{1j}, x_{2j}, \ldots, x_{nj}]$, $\beta_i = [\beta_{i1}, \beta_{i2}, \ldots, \beta_{im}]$ is the output weight, $u_j = [u_{1j}, u_{2j}, \ldots, u_{mj}]$, and $g(x)$ is the activation function. Equation (1) can be expressed in the matrix as

$$H\beta = U^T \tag{2}$$

where $U = [u_1, u_2, \ldots, u_Q]$, U^T is the transpose matrix of matrix U, $\beta = [\beta_1, \beta_2, \ldots, \beta_L]^T$, and H is the hidden layer output matrix, which can be expressed as

$$H = \begin{bmatrix} g(a_1 \cdot x_1 + b_1) & \cdots & g(a_L \cdot x_1 + b_L) \\ \vdots & \cdots & \vdots \\ g(a_1 \cdot x_Q + b_1) & \cdots & g(a_L \cdot x_Q + b_L) \end{bmatrix}_{Q \times L} \tag{3}$$

The ELM network is designed to minimize the error between the actual output and the desired output, allowing for the output weight β to be obtained by solving the least squares solution of the following equation

$$\min_{\beta} \left\| H\beta - U^T \right\| \tag{4}$$

The final solution of this equation is obtained as

$$\hat{\beta} = H^{+} U^T \tag{5}$$

H^{+} is the generalized inverse matrix of the output matrix H.

Firstly, the input weights and threshold b of the ELM network are randomly initialized, and the activation function is set. Then, the hidden layer output matrix H is computed. Finally, the output weight matrix β is calculated. In this process, random initialization of input weights and threshold can increase the randomness of the network and reduce the risk of overfitting. The activation function is used to increase the nonlinearity of the network, enabling it to handle more complex problems.

3.2. ASO Principle

ASO is a mathematical model that is based on the physical laws of motion governing atoms in molecular dynamics. It stimulates the displacement of atoms in a molecular system due to mutual and systemic binding forces [19]. The ASO algorithm assumes that atomic motion satisfies Newton's second law. Atoms experience two forces, one being the interaction forces generated by the Lennard-Jones potential and the other being the binding force generated by the atomic covalent bond.

The interaction force $F^d{}_i$ can be expressed as the sum of forces acting on the i-th atom by other atoms inside the molecule and can be written as

$$F_i^d(t) = \sum_{j \in N_{best}} rand_j F_{ij}^d(t) \tag{6}$$

where $rand_j$ is a random number distributed within [0,1], d is the number of dimensions in which the atoms are located, and N_{best} is the set of n atoms with good fitness function values. $F^d{}_{ij}(t)$ is the Lennard-Jones potential force acting on the i-th atom by the j-th atom at the current iteration number t and is defined as

$$F_{ij}^d(t) = -\eta(t)\left\{2\left[S_{ij}(t)\right]^{13} - \left[S_{ij}(t)\right]^{7}\right\} \tag{7}$$

$$S_{ij}(t) = \frac{r_{ij}(t)}{\sigma(t)} \tag{8}$$

Here, η is the depth function to adjust the repulsion region or the attraction, r_{ij} is the Euclidean distance between i atom and j atom, and $\sigma(t)$ is the length scale represented as

$$\sigma(t) = \left\| x_i(t), \frac{\sum_{j \in N_{best}(t)} x_j(t)}{N_{best}(t)} \right\|_2 \tag{9}$$

where x_i (x_j) is the position of $i(j)$ atom. To improve the exploration range, Equation (8) for calculating S_{ij} will be further modified accordingly to reference [18].

Taking into account the binding forces of G in covalent bonds to highlight the guiding role of the population's best atom, it is assumed that each atom has a covalent bond with the population's best atom. Therefore, each atom is subjected to the binding force of the best atom, which can be expressed as follows.

$$G_i^d = \lambda[x_{best}^d(t) - x_i^d(t)]e^{-20\frac{t}{T}} \tag{10}$$

where λ is the coefficient factor, $x^d{}_{best}(t)$ is the best atomic position of the population in the t-th iteration, $x^d{}_i(t)$ is the current position of the atom in the t-th iteration, and T is the total number of iterations.

The acceleration of the i-th atom with the mass of m_i under the action of the interaction and binding forces can be calculated as follows

$$a_i = (F_i + G_i)/m_i \tag{11}$$

In each iteration, the velocity and position of an i-th atom are updated based on the obtained acceleration as follows

$$\begin{aligned} v_i^d(t+1) &= rand_i^d v_i^d(t) + a_i^d(t) \\ x_i^d(t+1) &= x_i^d(t) + v_i^d(t+1) \end{aligned} \tag{12}$$

where $v^d{}_i$ is the velocity of the atom.

3.3. HBT Junction Temperature Prediction Model Based on ASO-ELM

The basic structure of the ELM predictive junction temperature model is presented in Figure 2, consisting of an input layer, a hidden layer, and an output layer. The input variables, V_c and I_c, are considered the key factors for predicting the maximum junction temperature. Although ELM has a fast learning speed, the forecast outcomes are subjected to the influence of random input weights and hidden layer deviations, leading to significant differences in the results of each model training.

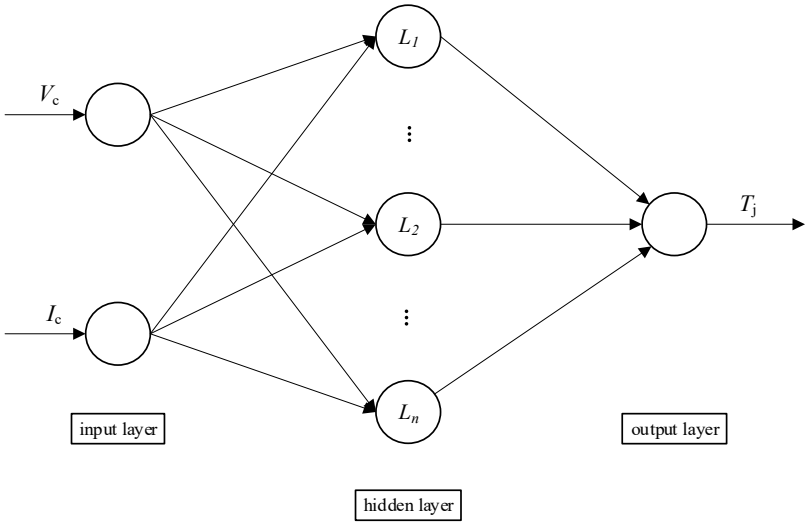

Figure 2. Network of ELM for junction temperature prediction.

In order to enhance the performance and prediction accuracy of the ELM model for predicting junction temperature, the ASO algorithm is utilized to optimize the initial parameters of ELM. Thus, the core of the maximum junction temperature prediction model proposed in this paper is to determine the optimal position of atoms through the optimization of the ASO algorithm. The position information includes the initial input weight and threshold of ELM. The ASO algorithm is employed to solve it iteratively until the optimal parameter combination is obtained. The optimized ELM model is then utilized to forecast the junction temperature. The steps for predicting the maximum junction temperature of ASO-ELM are as follows:

1. Conduct a temperature test on the HBT power cell to obtain T_j, V_c and I_c data and form a data set.

2. After removing abnormal data, use the maximum-minimum normalization method to eliminate the impact of data dimension and divide the normalized data into training data and test data.
3. Set the parameters of the ASO algorithm, such as the number of atoms in the population, the maximum number of iterations, dimensions, etc. Determine the topological structure of ELM and initialize the parameters of ELM.
4. Initialize the position and speed of atoms in the atomic population, take the output mean square error as a fitness function, calculate the fitness value of each atom, and record the current optimal position and optimal solution.
5. Calculate the acceleration, velocity and position of individual atoms, and update the objective function value of each atom.
6. Compare the objective function value of the updated space with that of the un-updated space. If the updated position is better, the value will be retained for the next search. Otherwise, it will be ignored.
7. Check whether the maximum number of searches has been reached. If yes, end the search and output the optimal solution to the next step. Otherwise, return to continue to perform step (5).
8. Establish the ELM model optimized based on the ASO algorithm. The optimal solution is the input weight and deviation value of the ELM model.
9. Input the sample into ELM with optimal combination parameters for testing, and obtain the predicted maximum junction temperature T_j after reverse normalization of the data.

The maximum junction temperature prediction process based on ASO-ELM is shown in Figure 3.

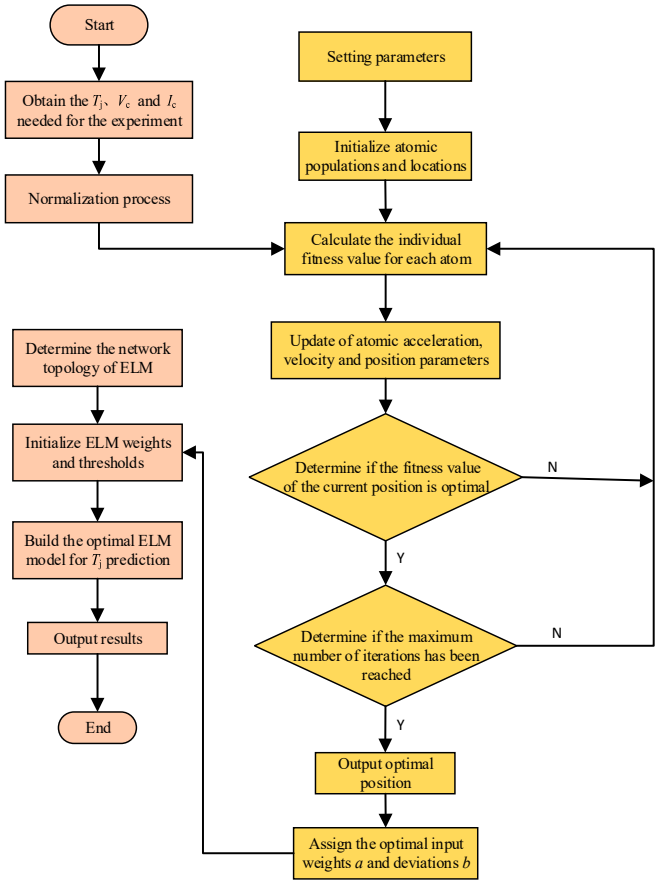

Figure 3. Flowchart of ASO-ELM model.

4. Results

In actual infrared temperature testing, a dataset of 293 sets of HBT power cell data was obtained for predicting the maximum T_j. The model's two input variables are V_c and I_c, while the output variable is T_j. The empirical formula indicates that the number of hidden layer neurons is 12, and the ELM model structure is 2-12-1 with the sigmoid activation function. MATLAB was used for the simulation. To demonstrate the advantages of the proposed model, it was compared with BPNN, ELM and GA-ELM. The models' parameters were set as follows: 50 iterations and a population size of 50 for ASO and GA, an ASO depth weight of 50, and a coefficient weight of 0.2. The GA crossover and mutation probabilities were set to 0.7 and 0.01, respectively. The optimal input weight and deviation matrix optimized by different algorithms were assigned to the ELM network, respectively. The model evaluation was based on absolute error (AE), mean absolute error (MAE), relative error (RE), and root mean square error (RMSE), which are defined as follows.

$$AE = |y_i - y_i^*| \tag{13}$$

$$MAE = \frac{\sum_{i=1}^{n} |y_i^* - y_i|}{n} \tag{14}$$

$$RE = \frac{|y_i - y_i^*|}{y_i} \times 100\% \tag{15}$$

$$RMSE = \sqrt{\frac{\sum_{i=1}^{n} (y_i^* - y_i)^2}{n}} \tag{16}$$

where n is the number of predicted samples, y_i is the measured data, and y_i* is the predicted value.

To demonstrate the validity of the prediction, junction temperature data at different bias voltages and currents were randomly selected for prediction. The prediction results based on ELM, GA-ELM, and ASO-ELM models are shown in Figure 4. The ELM model takes power consumption as an independent variable, while ASO-ELM and GA-ELM take V_c and I_c as independent variables. Figure 5 compares the absolute and relative errors of junction temperature prediction among the models. In some cases, the ELM model fails to guarantee the stability of performance, as shown by the steep slopes at the 8th and 21st sample points in Figure 5. In contrast, the error changes in the ASO-ELM model are much more stable, with the absolute error and relative error remaining within 2 °C and 2.3%, respectively. This indicates that the ELM prediction model optimized using ASO has a good fit, and the error fluctuation between the predicted and true values is small. By optimizing the selection of weights and thresholds of ELM using the ASO algorithm, the obtained model has good generalization, which can effectively solve the problem of the low generalization ability of the model due to the random generation of weights and thresholds of ELM.

Due to the randomness of the algorithm's results, the maximum junction temperature was predicted 100 times with ELM and tested 50 times with ASO-ELM and GA-ELM. BPNN was also added for comparison. The average error obtained was calculated in Table 1. The average MAE of ASO-ELM reached 1.7314, and the average RMSE of ASO-ELM was still the lowest at 1.9526. The test results demonstrated that the accuracy of the ELM model optimized by ASO has significantly improved the junction temperature prediction, effectively reducing the error of the basic ELM model and improving the prediction effect. Compared with the GA-optimized ELM junction temperature prediction model, the ASO model offers better prediction accuracy and less modeling time.

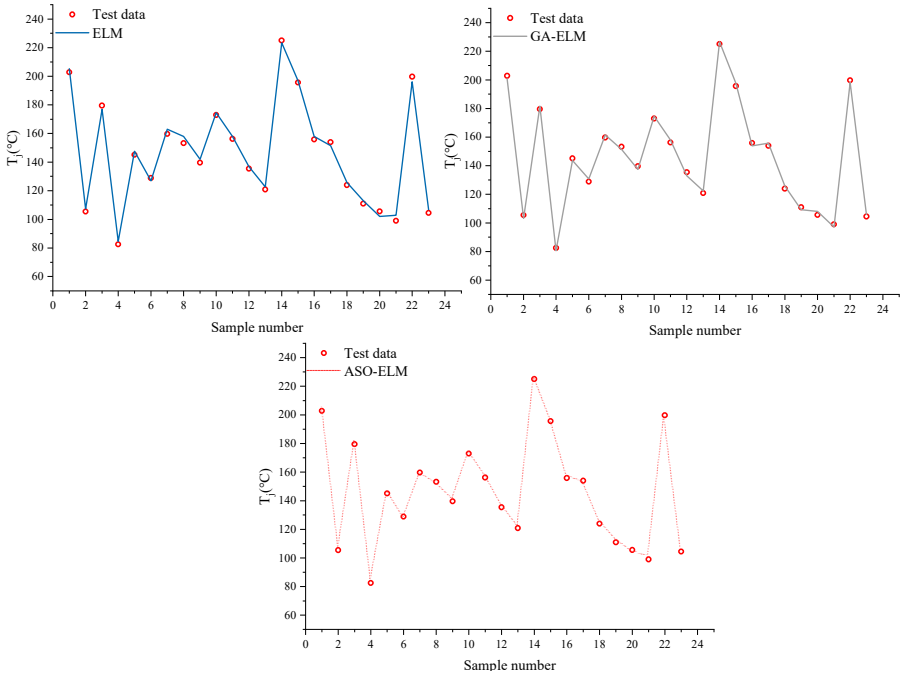

Figure 4. Prediction results of T_j by ELM model, GA-ELM model and ASO-ELM model.

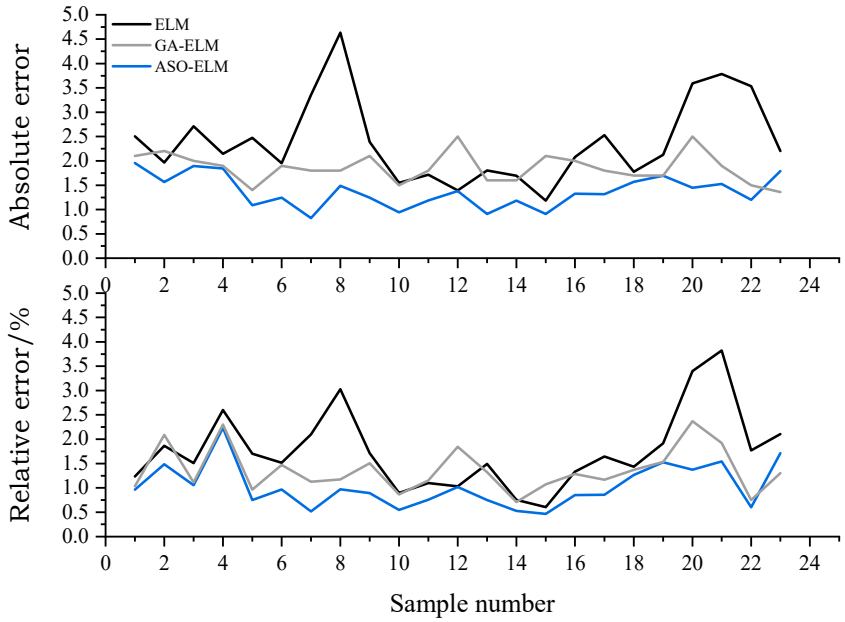

Figure 5. Absolute and relative errors of ELM model, GA-ELM model and ASO-ELM model.

Table 1. Performance index statistics of the four models.

Model	Index of Evaluation	Max (°C)	Min (°C)	AVE (°C)	Modeling Time (s)
ELM	MAE	8.3127	2.4817	4.6682	0.01480
	RMSE	24.1662	2.6441	12.513	
BPNN	MAE	3.8172	2.1596	2.5149	4.8413
	RMSE	4.4139	2.3237	2.6954	
GA-ELM	MAE	2.4633	1.9547	2.2976	22.1748
	RMSE	2.6512	2.1630	2.3423	
ASO-ELM	MAE	2.2583	1.3709	1.7314	8.7527
	RMSE	2.637	1.4077	1.9526	

In order to demonstrate the efficacy of our proposed temperature prediction model, we have selected eight groups of test data with varying voltage and current, all of which have been tested under the same power consumption conditions. These data sets were then predicted using the ASO-ELM model, and the comparison results are presented in Figure 6. The gray curve in the figure represents the actual QFI measurement data, while the square and triangle legends represent the maximum junction temperatures at 4 V and 5 V, respectively. The red curve in the figure depicts the temperature values obtained based on the ASO-ELM prediction. Results reveal that temperature values corresponding to different voltages and currents vary; thus, it is not appropriate to rely solely on power consumption as a factor to calculate thermal resistance and derive the junction temperature. The range of variation of predicted values based on ASO-ELM is similar to the values measured by QFI, indicating that our method is capable of predicting the maximum junction temperature of HBT accurately.

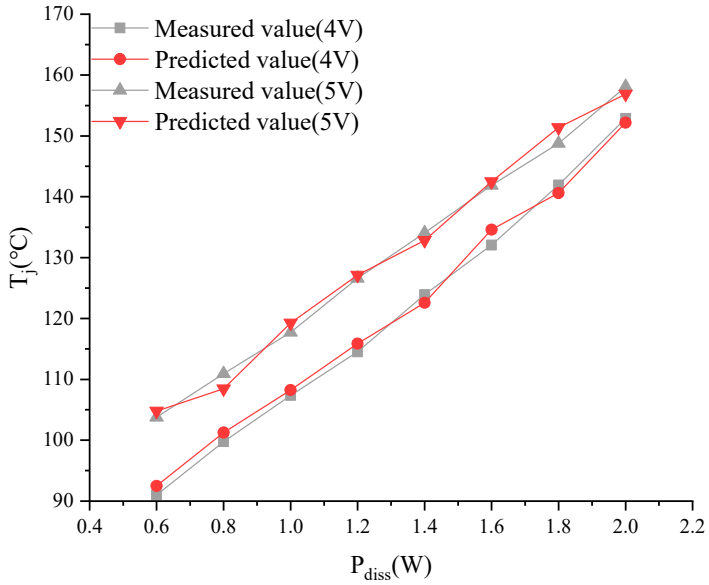

Figure 6. Comparison of junction temperature prediction at different voltages based on ASO-ELM (same power consumption conditions).

Therefore, the results indicate that the introduction of the ASO algorithm effectively optimized the ELM model and improved its prediction accuracy. The average MAE of the ASO-ELM model was reduced by 84.4%, 36.22%, and 24.64%, respectively, compared to the ELM, BPNN, and GA-ELM models. Additionally, the average RMSE of ASO-ELM was 62.9%, 27.56%, and 16.64% lower than ELM, BPNN, and GA-ELM, respectively. Therefore, the established ASO-ELM model outperforms other models in predicting the junction temperature.

5. Conclusions

In this paper, we propose a novel GaAs HBT maximum junction temperature prediction model that considers voltage and current as influencing factors. The model uses a machine-learning approach. It utilizes the ASO algorithm to optimize the input weight and hidden layer deviation of ELM, with bias voltage and collector current as inputs and maximum junction temperature as output. Experimental results demonstrate that the maximum junction temperature prediction model proposed in this paper is more rigorous compared to the model that only considers the effect of power consumption. The prediction results are obtained more quickly with the help of ASO-ELM. In future work, the proposed model can be utilized to analyze the temperature distribution of the entire power cell, providing guidance for device layout design and temperature compensation.

Author Contributions: Conceptualization, Y.Y. and X.S.; methodology, Y.Y.; software, C.Z.; validation, C.Z. and Y.Y.; formal analysis, X.S.; investigation, C.Z.; resources, X.S.; data curation, X.S.; writing—original draft preparation, X.S.; writing—review and editing, Y.Y.; visualization, Y.Y.; supervision, Y.Y.; project administration, C.Z.; funding acquisition, X.S. All authors have read and agreed to the published version of the manuscript.

Funding: This work was supported by the National Natural Science Foundation of China under "Project No. 61701333".

Data Availability Statement: Restrictions apply to the availability of this data. Information from Suzhou Innovation Technology Company, Ltd. (Suzhou, China) and provided by the author with permission from the company.

Conflicts of Interest: The authors declare no conflict of interest.

References

1. Nishihori, K.; Ishida, K.; Kitaura, Y.; Uchitomi, N. Thermal analysis of GaAs power monolithic microwave IC's mounted with epoxy attachment. *IEEE Trans. Compon. Packag. Manuf. Technol. Part A* **1997**, *20*, 220–224. [CrossRef]
2. Darwish, A.M.; Hung, H.A.; Bayba, A.J.; El-Kinawi, K. Accurate calculation of junction temperature of HBTs. *IEEE Trans. Microw. Theory Tech.* **2011**, *59*, 652–659. [CrossRef]
3. Ooi, B.L.; Chen, B.; Lin, F.; Kooi, P.S.; Hui, C.S. A fast and practical approach to the determination of junction temperature and thermal resistance for BJT/HBT devices. *Microw. Opt. Technol. Lett.* **2002**, *35*, 499–502. [CrossRef]
4. D'Alessandro, V.; Catalano, A.P.; Codecasa, L.; Zampardi, P.J.; Moser, B. Accurate and efficient analysis of the upward heat flow in InGaP/GaAs HBTs through an automated FEM-based tool and Design of Experiments. *Int. J. Numer. Model. Electron. Netw. Devices Fields* **2019**, *32*, e2530. [CrossRef]
5. Chakravorty, A.; D'Esposito, R.; Balanethiram, S.; Fregonese, S.; Zimmer, T. Analytic estimation of thermal resistance in HBTs. *IEEE Trans. Electron Devices* **2016**, *63*, 2994–2998. [CrossRef]
6. Darwish, A.M.; Bayba, A.J.; Khorshid, A.; Rajaie, A.; Hung, H.A. Calculation of the nonlinear junction temperature for semiconductor devices using linear temperature values. *IEEE Trans. Electron Devices* **2012**, *59*, 2123–2128. [CrossRef]
7. Melczarsky, I.; Lonac, J.A.; Filicori, F. Electrical measurement of the junction temperature and thermal resistance of HBTs. *IEEE Microw. Wirel. Compon. Lett.* **2006**, *16*, 78–80. [CrossRef]
8. Sun, X.D.; Zhang, X.D.; Sun, Y.F. Thermal characterization and design of GaAs HBT with heat source drifting effects under large current operating condition. *Microelectron. J.* **2020**, *100*, 104779. [CrossRef]
9. Wu, J.; Zhou, L.; Du, X.; Sun, P. Junction temperature prediction of IGBT power module based on BP neural network. *J. Electr. Eng. Technol.* **2014**, *9*, 970–977. [CrossRef]
10. Dou, Y. An improved prediction model of IGBT junction temperature based on backpropagation neural network and Kalman filter. *Complexity* **2021**, *2021*, 5542889. [CrossRef]
11. Iwamoto, M.; Xu, J.; Zhou, W.; Root, D.E. Knowledge-based neural network (KBNN) modeling of HBT junction temperature and thermal resistance from electrical measurements. In Proceedings of the 2017 IEEE MTT-S International Microwave Symposium, Honolulu, HI, USA, 4–9 June 2017; pp. 1069–1071.
12. Huang, G.B.; Zhu, Q.Y.; Siew, C.K. Extreme learning machine: Theory and applications. *Neurocomputing* **2006**, *70*, 489–501. [CrossRef]
13. Huang, G.; Huang, G.B.; Song, S.; You, K. Trends in extreme learning machines: A review. *Neural Netw.* **2015**, *61*, 32–48. [CrossRef] [PubMed]
14. Zhu, B.; Feng, Y.; Gong, D.; Jiang, S.; Zhao, L.; Cui, N. Hybrid particle swarm optimization with extreme learning machine for daily reference evapotranspiration prediction from limited climatic data. *Comput. Electron. Agric.* **2020**, *173*, 105430. [CrossRef]
15. Wang, S.; Zhang, J.; Liu, M.; Liu, B.; Wang, J.; Yang, S. Large-Signal Behavior Modeling of GaN P-HEMT Based on GA-ELM Neural Network. *Circuits Syst. Signal Process.* **2022**, *41*, 1834–1847. [CrossRef]
16. Zhao, W.; Wang, L.; Zhang, Z. A novel atom search optimization for dispersion coefficient estimation in groundwater. *Future Gener. Comput. Syst.* **2019**, *91*, 601–610. [CrossRef]
17. Tian, T.; Sun, X.H.; Gao, H.; Lu, S. Improved thermal management of power cells with adding cooling path from collector to ground. *Electron. Lett.* **2019**, *55*, 513–515. [CrossRef]
18. Ding, S.; Zhao, H.; Zhang, Y.; Xu, X.; Nie, R. Extreme learning machine: Algorithm, theory and applications. *Artif. Intell. Rev.* **2015**, *44*, 103–115. [CrossRef]
19. Zhao, W.; Wang, L.; Zhang, Z. Atom search optimization and its application to solve a hydrogeologic parameter estimation problem. *Knowl. Based Syst.* **2019**, *163*, 283–304. [CrossRef]